Properties of $((CH_3NH_3)_{1-x}Cs_x)_3Bi_2I_9$: (x=0-1.0) Hybrid Perovskite Solar Cells with Chlorobenzene Treatment

M.F. Achoi[1], S. Kato[2], N. Kishi[2] and T. Soga[2,*]

[1]*Faculty of Applied Sciences, Universiti Teknologi MARA, Cawangan Sabah, Kampus Kota Kinabalu, Sabah 88997, Malaysia*

[2]*Department of Electrical and Mechanical Engineering, Nagoya Institute of Technology, Nagoya, Aichi 466-8555, Japan*

Abstract: Hybrid-perovskite solar cells, a promising lead-free perovskite material, have been attracted for optoelectronic applications due to an excellent optical and electrical properties with low production cost. Herein, methylammonium bismuth iodide and cesium bismuth iodide were mixed to form hybrid structure for the improvement of photovoltaic properties, which were fabricated using all-solution processed multi-step spin coating technique with changing the composition, x, of CBI, $((CH_3NH_3)_{1-x}Cs_x)_3Bi_2I_9$; (x=0 – 1.0). Chlorobenzene was added to the solution to improve the surface morphology. By optimizing the composition of CBI in MBI, the morphology, structural and optical properties of HPeSCs have been improved. It showed that the morphology is homogeneous, compact and a uniform layer, while the crystallinity shows an improvement as well. The open circuit voltage, the short circuit current and the power conversion efficiency were much improved with using hybrid structure. Our study shows that the significance of the hybridization process gives a new route in fabricating a better active absorber layer of PeSCs in the future.

Keywords: Hybrid-perovskite solar cell, Pb-free, Bismuth, Spin coating, XRD, SEM.

1. INTRODUCTION

To date, the hybrid-perovskite solar cells (HPeSCs) have been attracted much attention from many researchers as Pb-free PeSCs with high stability [1, 2]. Recently, the combination of cesium-bismuth iodide (CBI, $Cs_3Bi_2I_9$) as an inorganic-based PeSCs and methylammonium- bismuth iodide (MBI, $MA_3Bi_2I_9$) as an organic-based PeSCs to form HPeSCs has been started getting attention. The combination of these two components is giving a promising in the improvement of thermal stability, optical and electrical properties [3]. CBI has a wide range of absorption and optical bandgap as reported by Johansson *et al.* and Oz *et al.* [4, 5] while MBI has absorption around 500 nm [6]. Besides, $MA_3Bi_2I_9$ is high carrier mobility [7] and non-toxic material [1], while CBI is having a long-term stability and high thermal stability [8]. Additionally, both compounds have a similarity in term of crystalline structure which having a zero-dimensional with isolated bioctahedrons and hexagonal structure. It thus gives an advantage for the hybridization process [9] In this regard, cesium and bismuth-based halide perovskite has emerged as an eco-friendly and non-toxic PeSCs device [10, 11]. Meanwhile, many efforts have been taken by previous researcher to improve the surface, structural, optical properties, and the performance of HPeSCs. For example, Oz *et al*. reported the combination of cesium with Pb, but the Pb is a toxic material and found many pinholes [5]. Unlu *et al*. studied the mixing between Cs^+ and MA^+, and found the grain morphology with an exciton absorption peak at 500 nm. Besides, Ma *et al*. reported the performance of Bi-PeSCs is influenced by the holes on the surface [12]. Then, Khadka *et al*. found poor surface morphology of Cs^+ based Bi-PeSCs [13]. However, to date, all those reports are still focusing on the improvement of perovskite morphology that might be detrimental to the performance of PeSCs. One way for the improvement is to fabricate $X_3Bi_2I_9$–type PeSCs by mixing the inorganic and organic-based components. But so far, such a Bi-based hybrid perovskite solar cell has not been reported very much. Herein, $(CH_3NH_3)_{1-x}Cs_x)_3Bi_2I_9$ (MCBI) HPeSCs that mixed $(CH_3NH_3)_3Bi_2I_9$ (MBI) and $Cs_3Bi_2I_9$ (CBI) with changing the composition from x = 0 to 1 with the entire range were evaluated. The purpose of this paper is to show the structural, optical and photovoltaic properties of HPeSCs and improve the solar cell performance with changing the composition.

2. EXPERIMENTAL METHODS

FTO substrates and TiO_2 solution were prepared according to our previous reported work [14, 15]. For preparation of MBI solution is referred to ref. [16] while for CBI solution, BiI_3 (Sigma-Aldrich, 99.999%) and CsI (Sigma-Aldrich, 99.999%) were mixed with ratio

*Address correspondence to this author at the Department of Electrical and Mechanical Engineering, Nagoya Institute of Technology, Nagoya, Aichi 466-8555, Japan; E-mail: soga@nitech.ac.jp

E-ISSN: 2410-2199/24

[1.5:1.0] in 10 mL of DMF to form a 0.5 M CBI solution. The mixed solution was then stirred on a hotplate and left for aging time. This step is repeated for the preparation of different volume of CBI solution. After aging time, the MBI and CBI solution were mixed according to different CBI fraction with x=0, x=0.2, x=0.5, x=0.8, and x=1.0. Next, the mixture of CBI and MBI is stirred again and left for aging time. Afterward, the mixture is spin-coated on the mp-TiO_2/c-TiO_2/FTO/glass at 1000 rpm for 30 s. Then, the fabricated sample is annealed at 100 ^oC for 10 min, and these steps are repeated for eight times to obtain eight layers of MBI/CBI perovskite. At intervals between each layer fabrication, one drop of chlorobenzene (CB) was dripped instantly while spinning at between 30 s and 35 s to improve the surface morphology. However, similar films without using CB treatment were also prepared for comparison. For preparation of P3HT film, 0.015 g of P3HT was dissolved in 1 mL dichlorobenzene and then left under continuous stirred for 24 h. Next, the P3HT is fabricated on the MBI/CBI/mp-TiO_2/c-TiO_2/FTO/glass at 3000 rpm for 20 s, followed by annealed at 120 ^oC for 15 min. The whole fabrication process was carried out in a dry nitrogen-filled glovebox. Finally, the colloidal graphite was spin-coated on top of the P3HT at 5000 rpm for 20 s and cooled in room temperature, followed by the deposition of Ag paste on colloidal graphite [17]. The whole process was repeated for different of CBI fraction at x=0, x=0.2, x=0.5, x=0.8 and x=1.

The crystalline phase and morphology of HPeSCs were examined by X-ray diffractometer (XRD) (Rigaku RINT-2100 diffractometer) and scanning electron microscopy (SEM) (JEOL JSM-7600F), respectively. The optical properties and the solar cells performance were characterized using UV-vis spectrophotometer (JASCO Model V-570) and the solar simulator under simulated solar light illumination (AM 1.5, 100 $mW.cm^{-2}$), respectively. The thickness was measured using the Dektak measurement (Veeco-Dektak150).

3. RESULTS AND DISCUSSION

Figure **1** indicates the XRD curves of HPeSCs for different composition x and all the CBI peak is same as reported by Unlu *et al*. [18]. The XRD pattern of $MA_3Bi_2I_9$ matches the hexagonal $P6_3/mmc$ space group [19] with preferred orientation along the (011) plane on mp-TiO_2 coated FTO substrate. This is similar and consistent with the hexagonal $Cs_3Bi_2I_9$ crystallizes in the hexagonal $P6_3/mmc$ group that indexed patterns in the JCPDS database (JCPDS No.23-0847). Both having a zero-dimensional structure with isolated bioctahedrons [9], in line with the recently reported results [20]. At x=0, two peaks of MBI is observed at 16.40^o [21] and 24.58$^{o2)}$ corresponding to (004) and (006) [22] lattice planes, respectively. It can be observed that the main-phase peak of CBI at 25.14^o (00-6)[18)] is increased in intensity as increasing the CBI composition except for x=0, which no CBI peak is observed. One peak of TiO_2 is observed at 25.37^o [23] and three of FTO peaks are observed at 26.82^o [24], 33.91^o [21], and 38.6^o [25]. The TiO_2 peak at 25.37^o [23] is higher than MBI peak at 24.58^o (006) as shown in Figure **1**(**a**).

The MBI peak at 24.58^o is low intensity than TiO_2 peak at 25.37^o [23] as shown in Figure **1**(**a**). The reason to this low intensity peak is due to the CB affected the formation of MBI layer at intervals between each layer fabrication of MBI via rapid precipitation with super saturation level, which resulted in the reduction of MBI solution since CB has properties of anti-solvent which immiscibility and miscibility [3]. Moreover, the MBI has properties of fast crystallization and low solubility in common solvents of BiI_3 [26, 27]. Thus, with the addition of CB, it reduces the solubility of the MBI in the precursor solution. As a proof, we can observe that the thickness of MBI shows much reduction from 368 nm to 188 nm for fabricated MBI with no CB and with CB, respectively, as shown in Figure **2**(**b**) and (**c**). An accordance to SEM images, Figure **3**(**a**) clearly depicted that the morphology was distorted compared to without CB as shown in SEM images of Figure **4**(**a**). Besides, the CB also affected the formation of MCBI layer for x=0.2, x=0.5, x=0.8 and x=1.0 via the reduction of the thickness of film as shown in Figure **2**(**b**) and (**c**). This figure shows 50% of thickness reduces for MBI film (x=0), whereas 39% (x=0.2), 18% (x=0.5), 14% (x=0.8) for MCBI films and for CBI film 12% reduces (x=1.0) after dripped with CB solution. Thus, it elucidates that the CB affected much the formation of MBI film compared to the MCBI and CBI film during the fabrication process. In brief, the CB on the formation of MCBI active layer affected the crystalline phase and film thickness of HPeSCs and as a result, it might influence the solar cells performance of HPeSCs that will be discussed further in the PV section.

Meanwhile, the crystallinity of MCBI is improved as introducing the CBI into MBI as shown in Figure **1**. Our explanation agrees well with Mariyappan *et al*., who reported that the peaks intensity and the crystallinity

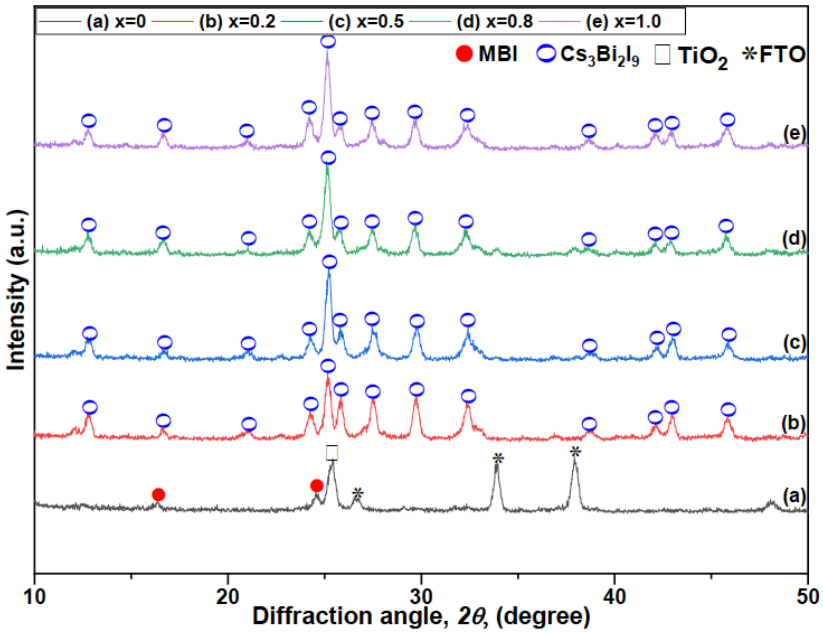

Figure 1: XRD curves of HPeSCs for different composition x.

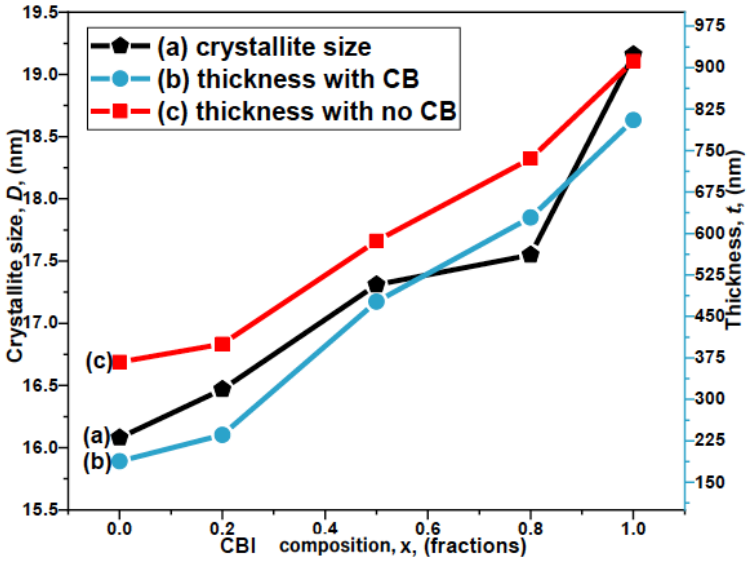

Figure 2: Crystallite size and thickness of the films for different composition x.

corresponding to CB treated CBI perovskite were improved [3]. Furthermore, we calculate the crystallites size, *D*, of HPeSCs using the Scherrer equation [24] and it increases as CBI composition increased as shown in Figure **2**(**a**). Likewise, the thickness of HPeSCs is increased as well as shown in Figure **2**(**b**) and (**c**). It thus elucidates that the CBI influences the *D*, crystallinity and thickness of HPeSCs with support of crystallization and thermal influences [19, 28]. The influences of the *D* and the thickness on the performance of the HPeSCs will be discussed in the photovoltaic section.

Figure **3** is the SEM images of HPeSCs with CB for different composition x. It shows the distribution of MBI particles (in red box) and it randomly distributed throughout mp-TiO_2 surface as confirmed by XRD in Figure **1**(**a**). It is clearly seen that the MBI particles are accumulated to each other form a bunch of an island-like structure and separated to each other. At x=0.2, with CBI induced into MBI, interestingly the morphology phase was totally changed with the formation of a small size of CBI particle with white color that uniformly distributed as confirmed by XRD result in Figure **1**(**b**) and it also confirmed that MBI peak is negligible as CBI

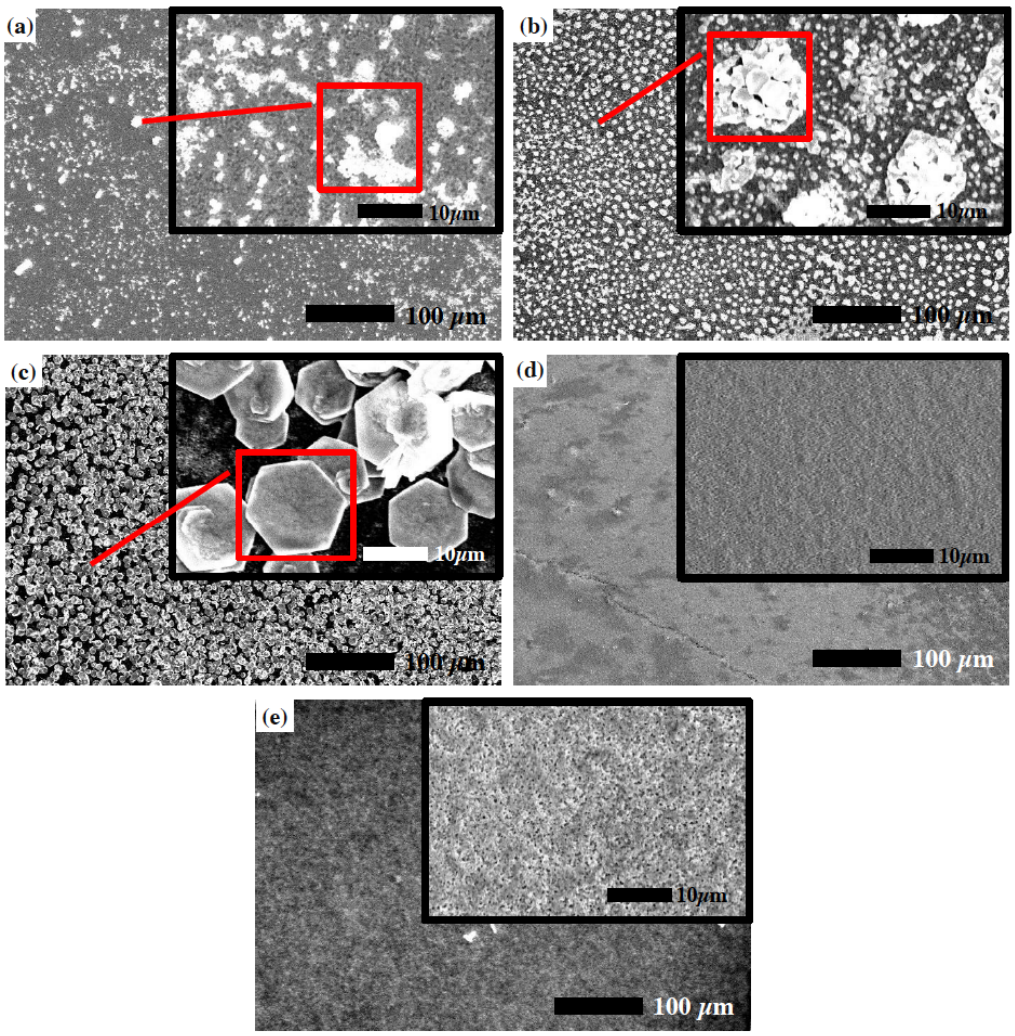

Figure 3: SEM images of HPeSCs for different composition x with CB.

peak starts to appear, which accumulated particle resulted in agglomeration as can be seen in the red box that separated to each other in Figure **3**(**b**). It means that the CBI phase starts to replace MBI phase as a main phase in HPeSCs. In accordance with XRD in Figure **1**(**b**), no TiO_2 peak is observed, and it elucidates that the surface of HPeSCs is well-covered. At x=0.5, interestingly it can be seen the formation of CBI hexagonal shape (in red box) is observed, that grew uniformly, close and overlapped to each other as shown in Figure **3**(**c**). Our hexagonal shape found is same as Ataei *et al.* and Ma *et al.* [12, 29]. This changing of morphological phase is encouraged by the nucleation growth process and assisted by supersaturation process [3]. However, at x=0.8 surprisingly it can be observed that the morphological phase absolutely changed and form a very smooth, uniform and homogeneous surface of HPeSCs in Figure **3**(**d**). No formation of hexagonal shape is observed this time. This happened due to the CB that changed the morphology of HPeSCs. Mariyappan *et al.* reported that the CB can effectively reduce the solubility of the solute in the precursor solution and drives the homogeneous nucleation due to the super-saturation process [3]. Previous study shows that using anti-solvent and no DMSO used resulting in homogeneous, pinhole-free and compact surface [3]. In this work, no DMSO and antisolvent of CB are used and it thus leads to a compact and homogeneous surface in our sample. According to Khadka *et al.* a uniform and compact film found in their sample after dripped with CB due to the nucleation process [3, 13]. The other reason is that multilayer of HPeSCs causes pinhole buried. Finally, at x=1.0 SEM visually depicts the compact and uniform surface as shown in Figure **3**(**e**). This might contribute to the better performance of HPeSCs that will be discussed in PV section.

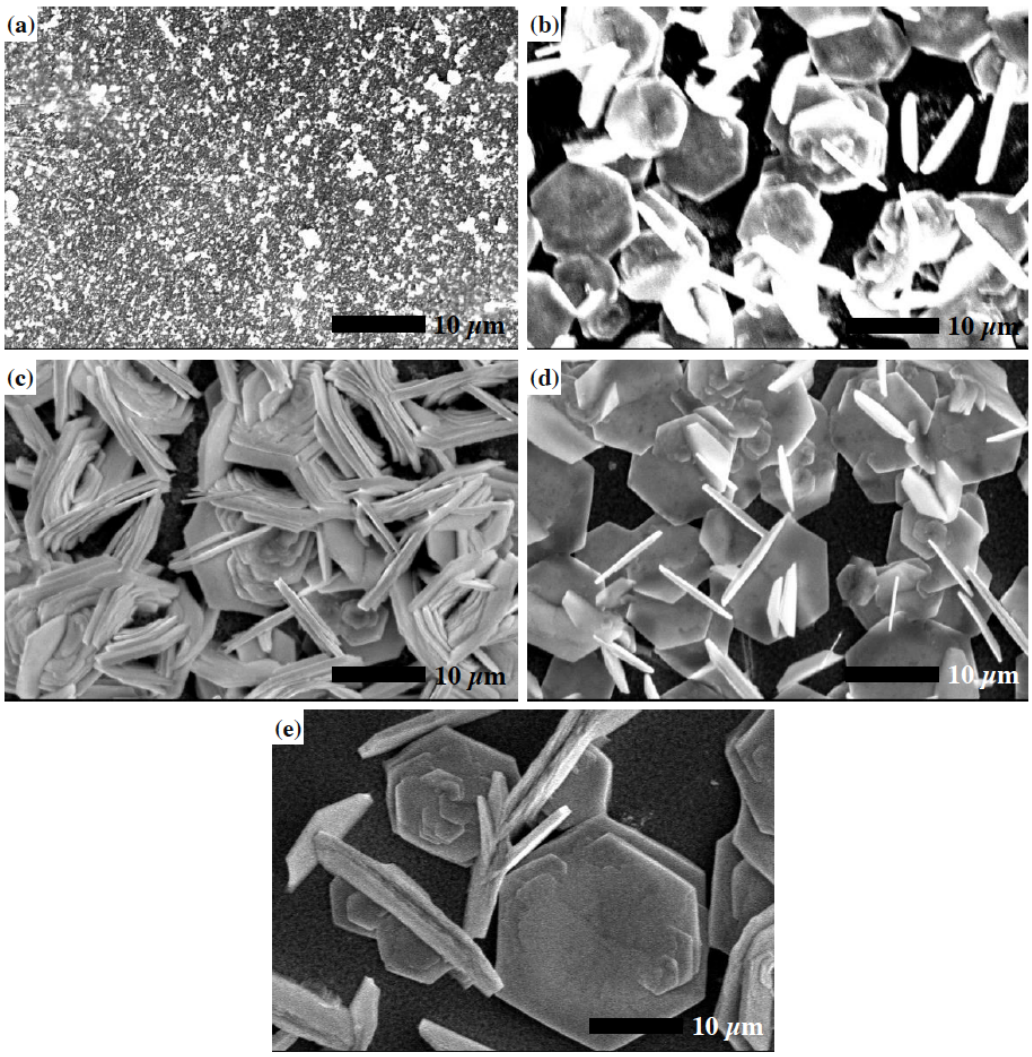

Figure 4: SEM images of HPeSCs for different composition x without CB.

On the other hand, the SEM morphology without CB treatment is also included in this study for comparison in Figure **4**. Generally, we can observe that all the SEM images did not present homogenous, smooth and uniform film without CB, the hexagonal shape still exist until CBI fraction at x=1.0. These SEM images without CB is relying with the thickness and photographed images of MCBI film that has been discussed earlier as shown in Figure **2**(**b** and **c**) and Figure **3**. It thus elucidates that the CB affected much the morphology of MCBI and it proves that the significance of CB usage to fabricating smooth, homogeneous, uniform and pinhole-free film.

Figure **5** exhibits absorption spectra of HPeSCs with CB for different composition x. The tauc plot is shown in the inset. At x=0, it can be observed that the optical bandgap, E_g, is 2.1 eV. However, after the incorporation of CBI into MBI, the optical bandgap is changed, which for 0.2≤x≤1.0, the E_g, is between 1.96 ~ 2.00 eV. It means that it becomes smaller with CBI composition, x. This is matching with the XRD result as shown in Figure **1**. Additionally, it can be observed that the extended absorption towards visible region as shown in Figure **1**(**d**) and (**e**). Our result is same as reported by Khadka *et al*. [13] that shows an extended-absorption and change of E_g. Besides, Mariyappan *et al*. reported also similar extended-absorption [3]. This changing of spectrum region is due to the influence of CBI in MBI [4, 5].

Figure **6** shows the performance of HPeSCs and Table **1** is a summary of the solar cell parameters, while inset is the schematic diagram of HPeSC design. In brief, with increasing CBI composition, the efficiency and V_{oc} of 0.0002 % and 0.09V were much increased to 0.01 % and ~0.59V, respectively from x=0 to x=0.8. However, at x=1.0, the efficiency and V_{oc} are

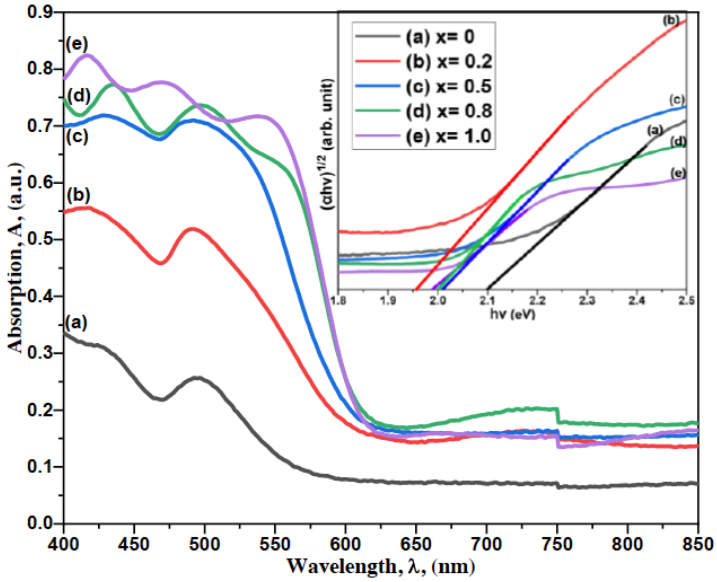

Figure 5: Absorption spectra of HPeSCs for different composition x. Inset is Tauc's plot of HPeSCs films.

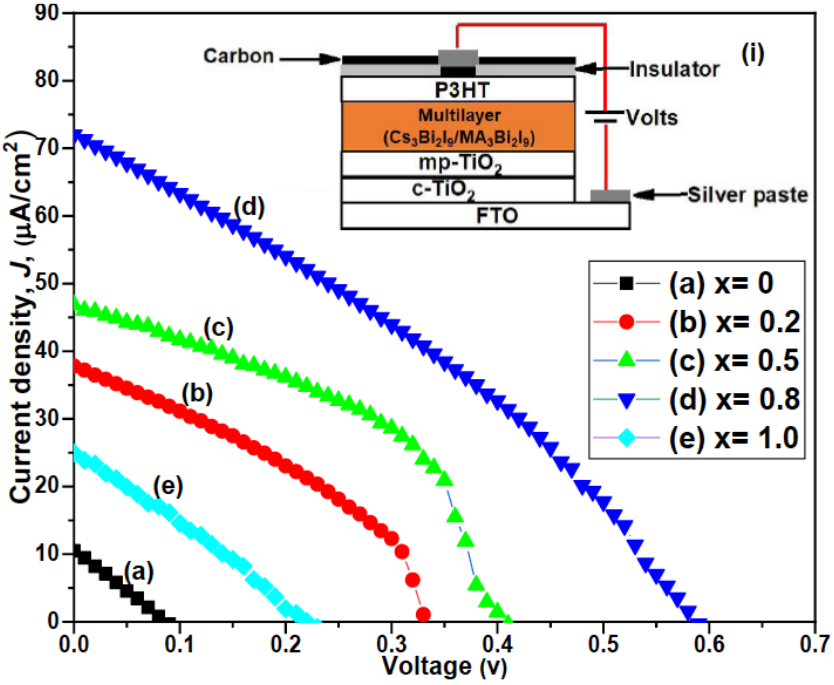

Figure 6: Current-voltage characteristics of HPeSCs for different composition x. The inset figure is the schematic diagram of HPeSCs design.

decreased instead, as shown in Figure **6**(**e**). The reason for this decrement will be further explained in the next paragraph. It clearly elucidates that the CBI significantly influenced the trend of this increment. According to Unlu *et al*. CBI incorporated into MBI showed an increment of V_{oc} [18]. In the case of our sample, a better crystallinity and a uniform surface morphology as shown in Figure **1**(**d**) and **3**(**d**-**e**), respectively, are identified as one of the factors that contributed to this increment. Correspondingly, the antisolvent of CB is identified to cause this improvement as reported by Mariyappan *et al*. [3]. Our explanation agrees well with the finding of Ataei *et al*., that the better morphology improved the interface contact and resulted in higher V_{oc} [29].

Furthermore, the *D* and the thickness influence the performances of HPeSCs as discussed early in the

Table 1: Photovoltaic Properties, Crystallite Size and Thickness of HPeSCs for Different Composition x

CBI fractions, x	J_{sc} (μA/cm^2)	V_{oc} (V)	FF (%)	PCE (%)	Crystallite size, *D* (nm)	Thickness, *t* (nm)
(a) x = 0	11	0.09	25.4	0.00023	16.1	188
(b) x = 0.2	38	0.33	37.2	0.00468	16.5	236
(c) x = 0.5	47	0.41	34.4	0.00876	17.3	477
(d) x = 0.8	72	0.59	31.8	0.0135	17.6	629
(e) x = 1.0	25	0.22	28.5	0.00157	19.2	805

XRD section. In the case of x=1.0, in comparison with the *D* value between MBI (x=0) and CBI (x=1.0) in Table **1**(**a**) and (**e**). It elucidates that an increment of the thickness is clearly influenced by the *D* of CBI as increasing the CBI composition in MBI as shown in Figure **2**(**a**) and (**b**). Hence, it affects the performance of HPeSCs, especially the J_{sc} and V_{oc} at x=1.0 as shown in Figure **6**. It shows that the performance of HPeSCs were dropped significantly and the Dektak measurement shows that the thickness is 805 nm for x=1.0. It thus causes the slow carrier mobility in an active layer producing low J_{sc} and V_{oc} values. According to Miller and Bernechea, the carrier mobility is slow due to the thicker film [30]. Besides, Xiao *et al*. reported that a too-large perovskites thickness causes reduced V_{oc} [31]. Additionally, Unlu *et al*. reported a thicker layer regardless of uniformity of perovskite layer that might be detrimental for efficient charge transport [18]. It thus elucidates that the performance of HPeSCs is not only influenced by the uniformity but also influenced by the thickness of perovskite layer.

4. CONCLUSIONS

HPeSCs were successfully fabricated by spin coating with changing the CBI composition in MCBI. The introduction of CBI into MCBI has significantly improved the properties of HPeSCs in terms of crystallinity, surface morphology, optical properties, and the performance. The HPeSCs show the homogeneous, compact and uniform surface, and the crystallinity of perovskite layer were improved. An optical property shows an extended -absorption spectrum at 620 nm while the max solar cell performance was attainable at x=0.8 of CBI with the best V_{oc} of 0.59V. Additionally, we found that the dripping of CB onto the surface of MCBI significantly influenced the changing of morphological phase, and key to fabricating a smooth, homogenous, compact and pinhole-free film, and to improve the crystallinity of the HPeSCs. At the end, our work may contribute a new idea towards designing a better absorber layer and develop a new generation of PeSCs via hybridization process in future.

REFERENCES

[1] Lyu M, Yun J, Cai M., Jiao Y, Bernhardt PV, Zhang M, Wang Q, Du A, Wang H, Liu G, and Wang L, Nano Res. 2016; 9: 692-702. https://doi.org/10.1007/s12274-015-0948-y

[2] Hoye RLZ, Brandt RE, Osherov A, Stevanovic V, Stranks SD, Wilson MWB, Kim H, Akey AJ, Perkins JD, Kurchin RC, Poindexter JR, Wang EN, Bawendi MG, and Bulovic V, Chem. Eur. J. Commun. 2016; 80401: 2605-2610. https://doi.org/10.1002/chem.201505055

[3] Mariyappan Chowdhury PTH, Subashchandran Bedja SI, Ghaithan HM, and Islam A, Sustain. Energy Fuels 2020; 4: 5042-5049. https://doi.org/10.1039/D0SE00786B

[4] Johansson MB, Zhu H, and Johansson EMJ, J. Phys. Chem. Lett. 2016; 7: 3467-3471. https://doi.org/10.1021/acs.jpclett.6b01452

[5] Öz S, Jena AK, Kulkarni A, Mouri K, Yokoyama T, Takei I, Ünlü F, Mathur S, and Miyasaka T, ACS energy Lett. 2020; 5: 1292-1299. https://doi.org/10.1021/acsenergylett.0c00244

[6] Sanders S, Stümmler D, Pfeiffer P, Ackermann N, Simkus G, Heuken M, Baumann PK, Vescan A, and Kalisch H, Sci. Rep. 2019; 9: 9774. https://doi.org/10.1038/s41598-019-46199-4

[7] Riley EB, Vladan S, David SG, and Tonio B, MRS Comm. 2015; 5: 265-275. https://doi.org/10.1557/mrc.2015.26

[8] E. B. Rachel EB, Daniel JS, Tomas L, Andrea RB, Rebecca AB, William HN, George FB, Eric TH, and Michael DM, J. Phy. Chem. Lett. 2016; 7: 746-751. https://doi.org/10.1021/acs.jpclett.6b00002

[9] Park BW, Philippe B, Zhang X, Rensmo H, Boschloo G, and Johansson EMJ, Adv. Mater. 2015; 9: 6806-6813. https://doi.org/10.1002/adma.201501978

[10] McClure ET, Ball MR, Windl W, and Woodward PM, ChemInform. 2016; 47. https://doi.org/10.1002/chin.201620017

[11] Sano Y, Satoh H, Chiba M, Okamoto M, Serizawa K, Nakashima H, and Omae K, J. Occup. Health. 2005; 47: 293-298. https://doi.org/10.1539/joh.47.293

[12] Ma Z, Peng S, Wu SY, Fang X, Chen X, Jia X, Zhang Yuan KN, Ding J, and Dai N, Phys. B Condens. Matter. 2017; 526: 136-142. https://doi.org/10.1016/j.physb.2017.08.079

[13] Khadka DB, Shirai Y, Yanagida M, and Miyano K, J. of Materials Chemistry 2019; C. 7: 8335-8343. https://doi.org/10.1039/C7TC02822A

[14] Achoi MF, Soga T, Rusop M, and Abdullah S, Curr. Nanomater. 2021; 6: 1-6. https://doi.org/10.2174/2405461506666210412153511

[15] Achoi MF, Noman MAA, Kato S, Kishi N, and Soga T, Materialia 2021; 16: 101077. https://doi.org/10.1016/j.mtla.2021.101077

[16] Achoi MF, Aiba S, Kato S, Kishi N, and Soga T, Mater. Lett. X. 2021; 12: 100096. https://doi.org/10.1016/j.mlblux.2021.100096

[17] Matiur RM, Kato S, and Soga T, J. Mater. Sci. Mater. Electron. 2021; 32: 18342-18350. https://doi.org/10.1007/s10854-021-06375-7

[18] Ünlü F, Kulkarni A, Lê AK, Bohr C, Bliesener A, Öz SD, Jena AK, Ando Y, Miyasaka T, Kirchartz T, and Mathur S, J. Mater. Res. 2021; 36: 1794-1804. https://doi.org/10.1557/s43578-021-00155-z

[19] Eckhardt K, Bon V, Getzschmann J, Grothe J, Wisser FM, and Kaskel S, Chem. Commun. 2016; 52: 3058-3060. https://doi.org/10.1039/C5CC10455F

[20] Abulikemu M, Sam OC, Miao X, Alarousu E, Murali B, Ndjawa GON, Barbé C, Labban AE, Amassian A, and Gobbo SD, J. Mater. Chem. A. 2016; 4: 12504-12515. https://doi.org/10.1039/C6TA04657F

[21] Sanders S, Stümmler D, Pfeiffer P, Ackermann N, Simkus G, and Heuken M, Baumann PK, Vescan A, and Kalish H, Phys. Status Solidi A. 2018; 23: 1800409. https://doi.org/10.1002/pssa.201800409

[22] Stümmler D, Sanders S, Mühlenbruch S, Pfeiffer P, Simkus Heuken GM, Vescan A, and Kalisch A, Phys. Status Solidi Appl. Mater. Sci. 2019; 216: 1900169. https://doi.org/10.1002/pssa.201900169

[23] Wang H, Tian J, Jiang K, Zhang Y, Fan H, Huang J, Yang LM, Guan B, and Song Y, RSC Adv. 2017; 7: 43826-43830. https://doi.org/10.1039/C7RA07123J

[24] Shirahata Y, J. Ceram. Soc. Japan. 2020; 128: 298-303. http://doi.org/10.2109/jcersj2.19156

[25] Wang Y, Liu Y, Xu Y, Zhang C, Bao H, and Wang J, Electrochem. Acta. 2020; 329: 135173. https://doi.org/10.1016/j.electacta.2019.135173

[26] Öz S, Hebig JC, Jung E, Singh T, Lepcha A, Olthof S, Flohre J, Gao Y, German R, Loosdrecht PHMV, Meerholz K, Kirchartz T, and Mathur S, Sol. Energy Mater. Sol. Cells. 2016; 158: 195-201. https://doi.org/10.1016/j.solmat.2016.01.035

[27] T. Singh, A. Kulkarni, M. Ikegami, and T. Miyasaka, ACS Appl. Mater. Interfaces. 2016; 8: 14542-14547. https://doi.org/10.1021/acsami.6b02843

[28] Saliba M, Matsui T, Seo JY, Domanski K, Correa-Baena JP, Nazeeruddin MK, Zakeeruddin SM, Tress W, Abate A, Hagfeldt A, and Grätzel M, Energy Environ. Sci. 2016; 9: 1989-1997. https://doi.org/10.1039/C5EE03874J

[29] Ataei M, Adelifard M, and Hosseini SS, J. Electron. Mater. 2021; 50: 571-579. https://doi.org/10.1007/s11664-020-08580-2

[30] Miller NC, and Bernechea M, APL Mater. 2018; 6: 084503. https://doi.org/10.1063/1.5026541

[31] Xiao Z, Bi C, Shao Y, Dong Q, Wang Q, Yuan Y, Wang C, Gao Y, and Huang J, Energy Environ. Sci. 2014; 7: 2619-2623. https://doi.org/10.1039/C4EE01138D

Received on 07-05-2024 Accepted on 24-05-2024 Published on 31-05-2024

DOI: https://doi.org/10.31875/2410-2199.2024.11.05